



**HAL**  
open science

## Development of a complex parent-metabolite joint population pharmacokinetic model.

Julie Bertrand, Céline M. Laffont, France Mentré, Marylore Chenel,  
Emmanuelle Comets

► **To cite this version:**

Julie Bertrand, Céline M. Laffont, France Mentré, Marylore Chenel, Emmanuelle Comets. Development of a complex parent-metabolite joint population pharmacokinetic model.. *Aaps Journal - Electronic Edition*-, 2011, 13 (3), pp.390-404. 10.1208/s12248-011-9282-9 . inserm-00606915

**HAL Id: inserm-00606915**

**<https://inserm.hal.science/inserm-00606915>**

Submitted on 7 Jul 2011

**HAL** is a multi-disciplinary open access archive for the deposit and dissemination of scientific research documents, whether they are published or not. The documents may come from teaching and research institutions in France or abroad, or from public or private research centers.

L'archive ouverte pluridisciplinaire **HAL**, est destinée au dépôt et à la diffusion de documents scientifiques de niveau recherche, publiés ou non, émanant des établissements d'enseignement et de recherche français ou étrangers, des laboratoires publics ou privés.

# Development of a complex parent-metabolite joint population pharmacokinetic model

Julie Bertrand<sup>1</sup>, Céline M. Laffont<sup>2</sup>, France Mentré<sup>1</sup>, Marylore Chenel<sup>3</sup>, Emmanuelle Comets<sup>1</sup>

<sup>1</sup> UMR738, INSERM, Paris, France; Université Paris Diderot, Paris, France

<sup>2</sup> UMR181, Physiopathologie et Toxicologie Expérimentales INRA, ENVT, Toulouse, France

<sup>3</sup> Institut de Recherches Internationales Servier, Courbevoie, France

**Running head:** Complex parent-metabolite PK model

Corresponding author: Julie Bertrand, UMR 738, INSERM, Université Paris Diderot, 16 rue Henri  
Huchard, 75018 Paris, France; telephone: 33 (0)1 57 27 75 39; fax: 33 (0)1 57 27 75 21; e-mail:  
julie.bertrand@inserm.fr

# ABSTRACT

This study aimed to develop a joint population pharmacokinetic model for an antipsychotic agent in development (S33138) and its active metabolite (S35424) produced by reversible metabolism. Because such a model leads to identifiability problems and numerical difficulties, the model building was performed using the FOCE-I and the SAEM estimation algorithms in NONMEM and MONOLIX, respectively. Four different structural models were compared based on Bayesian information criteria. Models were first written as ordinary differential equations systems and then in closed form (CF) to facilitate further analyses. The impact of polymorphisms on genes coding for the CYP2C19 and CYP2D6 enzymes respectively involved in the parent drug and the metabolite elimination were investigated using permutation Wald test. The parent drug and metabolite plasma concentrations of 101 patients were analyzed on two occasions after 4 and 8 weeks of treatment at 1, 3, 6 and 24 hours following daily oral administration. All configurations led to a two compartment model with back-transformation of the metabolite into the parent drug and a first-pass effect. The elimination clearance of the metabolite through other processes than back-transformation was decreased by 35 [9-53] % in *CYP2D6* poor metabolizer. Permutation tests were performed to ensure the robustness of the analysis, using SAEM and CF. In conclusion, we developed a complex joint pharmacokinetic model adequately predicting the impact of *CYP2D6* polymorphisms on the parent drug and its metabolite concentrations through the back-transformation mechanism.

**Key words:** Nonlinear mixed effects modeling, First-pass metabolism, Back-transformation mechanism, Estimation algorithms, Genetic covariate

# INTRODUCTION

For most drugs undergoing biotransformation, the process results in the formation of a more  
35 polar metabolite that is pharmacologically inactive and is eliminated more rapidly than the parent  
drug (1). For some drugs however, the metabolite may be pharmacologically active and/or produce  
adverse effects. Joint pharmacokinetic (PK) modelling accounts for the uncertainties in the data  
and allows feedback from the metabolite data to the parent drug data to influence the estimation.  
Thus, more and more studies now use this approach (2–4). Also, joint modelling allows to correctly  
40 evaluate and predict the impact of drug-drug interactions, and in the case of reversible metabolic  
systems, it is the only way to properly assess covariate effects.

However, such models can rapidly gain in complexity and present parameter identifiability  
problems and numerical difficulties in terms of estimation. To solve the issue of structural  
identifiability, it is important to identify the parameters or "apparent" parameters that can be  
45 estimated (3), and for the sake of parameter interpretation or covariate analysis, it might be  
needed to make some assumptions on the parameters (e.g. fixing one parameter to a given  
value) (4). Also, instability during the estimation is likely to result in solutions at local minima  
which may lead to biased parameter estimates and potentially wrong conclusions. Furthermore,  
numerical issues are likely to arise depending on the algorithms used for estimation in nonlinear  
50 mixed effect models (NLMEM). The First Order Conditional Estimation with Interaction (FOCE-  
I) algorithm (5) which is implemented in the NONMEM software (6), has been shown to  
encounter numerical difficulties even on simple single response models (7, 8). Yet, more robust  
alternatives have been proposed that avoid simplifying the equation for the likelihood, such as the  
Stochastic Approximation Expectation Maximization (SAEM) algorithm (9) implemented in the  
55 MONOLIX (10) and S-ADAPT (11) software. The NONMEM software remains though the most  
popular tool in population PK analysis because of its superior flexibility in the pharmaceutical  
field with tools such as NMTRAN. MONOLIX was only recently provided with a similar  
model translator called MLXTRAN. Of note, the SAEM algorithm was recently implemented  
in NONMEM software version 7.2.

60 During its development, an innovative antipsychotic agent from SERVIER research, the

S33138 (12), was shown to produce a metabolite which was also an active compound, called S35424, through hydrolytic cleavage by hydrolases, as assessed in human microsomes. Preclinical studies in rat and monkey supported the existence of a back-transformation of the metabolite into the parent drug, and this was further confirmed in a microdose study in man. Such reversible metabolism explained why both compounds showed similar terminal plasma half-life although the parent compound only slightly accumulates while the metabolite accumulates to a much larger extent (AUC accumulation ratio of 3). In addition to hydrolases, other metabolism pathways were identified for the parent drug involving CYP3A4 and to a lesser extent CYP2C19. The active metabolite was mainly metabolized through CYP2D6. Both CYP2C19 and CYP2D6 are encoded by highly polymorphic genes and these polymorphisms are known to have an impact on the course of many therapeutic drugs (13). Therefore, the effects of *CYP2D6* and *CYP2C19* polymorphisms on the PK of the parent compound and the metabolite were investigated in a phase II study using NLMEM. Drug plasma concentrations profiles were documented in patients at two occasions for the parent drug and its metabolite along with genotypes for five polymorphisms of the *CYP2D6* gene and two polymorphisms of the *CYP2C19* gene. In previous works, we have shown through simulations that asymptotic tests to detect a gene effect in NLMEM require a correction for type I error inflation on designs with unbalanced genotypes and/or including a small number of subjects (8, 14). This slight inflation can be handled by permutation tests (15). However such computing intensive approaches require a fast estimation method, all the more when the structural and variability models become complex.

The aim of the present work was thus to develop a joint population PK model for the antipsychotic and its metabolite after oral administration based on the data of the phase II study and to test for genetic effects. Because of the model complexity (reversible metabolism), the building of the model was performed using FOCE-I in NONMEM and SAEM in MONOLIX, in parallel. Furthermore, in order to alleviate the computational burden of permutation tests in the analysis of the genetic effect of *CYP2D6* and *CYP2C19* polymorphisms, models were encoded in ordinary differential equations (ODE) system and closed form solutions (CF). Finally, both internal and external model evaluations were performed, the latter using the data from a phase I

study. It is noteworthy that external evaluation provides the most stringent method for assessing  
90 the predictive ability of the developed model (16).

## MATERIALS AND METHODS

### *Pharmacokinetic studies*

The data used for model building came from a pilot, phase II, international, multicentre, randomized, double-blind, parallel-group, study assessing the effect of the above-mentioned  
95 antipsychotic drug compared to a gold-standard medication. In this study, one hundred and twenty patients were randomly allocated to 4 groups receiving for 8 weeks either 5, 10 or 20 mg of the novel antipsychotic or the gold standard medication (risperidone). Both treatments were administered orally and once a day in the morning before breakfast. Four blood samples were collected on two occasions, i.e. four and eight weeks after treatment initiation (W4 and W8). The  
100 sampling times were set empirically as the following: prior to drug administration and then 1, 3 and 6 h after drug administration. On the day of the sampling, the date and exact time of each blood sample were reported along with the date and exact time of the drug administration as well as those of the previous administration. Those exact times were used for the modelling.

For the external model evaluation, we used the data from a phase I randomized, double-blind  
105 tolerance study versus placebo with repeated increasing oral doses. Thirty healthy male volunteers were randomly divided into three groups: in each group, eight subjects received repeated once-a-day oral administrations of the parent drug at the dose of 10, 20 or 30 mg respectively, while two other subjects received the placebo. In this study, blood concentrations were documented at steady-state after 14 days of treatment with the following sampling times: prior to drug administration and  
110 then 0.33, 0.66, 1, 1.5, 2, 3, 4, 8, and 12 hours after drug administration. The exact times of blood collection were also recorded.

## ***Concentration measurements and genetic polymorphisms***

In both studies, the plasma concentrations of the antipsychotic and its active metabolite were determined using a validated method involving solid phase extraction followed by reverse phase  
115 Liquid Chromatography with Mass Spectrometry - Mass Spectrometry detection (LC/MS-MS). The intra/inter-day accuracy were 97.8/101.7% for the parent drug and 93/101.3% for the metabolite, the intra/inter-day precision were 4.7/5.6% for the parent drug and 6.1/8.6% for the metabolite and the recovery was 71% for the parent and 65.4% for the metabolite. Typical retention times of the chromatography were about 1.6 min for S33138 and the internal standard  
120 and 2.0 min for S35424, respectively. The limits of quantification were 0.56 and 0.44 nmol.L<sup>-1</sup> for the parent drug and its metabolite, respectively.

In the phase II study, blood samples were taken at the selection visit in order to determine the patient's genotype of *CYP 2D6*\*3, \*4, \*6, \*7, and \*8 alleles and of *CYP 2C19*\*2 and \*3 alleles while in the phase I study, a phenotyping test (dextrometorphan administration) was performed at  
125 the selection visit to ensure that all the persons involved were *CYP2D6* intermediate or extensive metabolizers. All samples were stored at -20°C and blood samples of included patients were sent on a regular basis to a central laboratory for analysis.

## ***Joint pharmacokinetic model***

Here, we present the analysis of concentration-time profiles from patients treated with the novel  
130 antipsychotic only (excluding patients treated with the reference medication). Concentrations were expressed in nmol.L<sup>-1</sup> for the joint modelling of the parent drug and its metabolite; molecular weights were respectively: 319.4 g.mol<sup>-1</sup> and 361.4 g.mol<sup>-1</sup>. Data below the limit of quantification as well as concentrations considered as non reliable given time or dosing information were treated as missing data and were excluded from the analysis.

135 Four different structural models of increasing complexity were investigated: their structural representations are shown in Figure 2 along with the definition of related parameters. The first model, on the left end of Figure 2, is a two compartment model where the dose is absorbed into the parent compartment at a rate  $K_{ap}$  and the parent drug (S33138) is either eliminated from the

system with a clearance  $CL_{po}$  or is transformed with a clearance  $CL_{pm}$  into a metabolite (S35424)
   
 140 which is eliminated from the system with a clearance  $CL_{mo}$ . Panhard *et al.* used such a model
   
 to jointly analyze nelfinavir and M8 concentrations (3). In the second model from the left on
   
 Figure 2, S35424 can in addition be transformed back to the parent with a clearance  $CL_{mp}$ . The
   
 existence of a back-transformation of S35424 into S33138 was supported by preclinical studies
   
 in rat and monkey and further confirmed in a microdose study in man. This microdose study
   
 145 included five healthy volunteers in a cross-over design where they received an oral dose of S33138
   
 plus an additional intravenous dose of  $C^{14}$ S35424 or  $C^{14}$ S33138 depending on the period with two
   
 groups of sequence composed of three and two subjects, respectively. Substantial concentrations
   
 of  $C^{14}$ S33138 were measured after administration of  $C^{14}$ S35424. Moreover, back-transformation
   
 of the metabolite into the parent drug is a well known process for numerous amines. A similar
   
 150 model was used to describe the increased hydrolysis of tesaglitazar metabolite into tesaglitazar via
   
 biliary circulation in renally impaired subjects (17). In the third model from the left on Figure 2,
   
 a first-pass effect has been considered: the dose not only enters into the parent compartment at a
   
 rate  $K_{ap}$  but also enters into the metabolite compartment at a rate  $K_{am}$ . This model, although
   
 less physiological, is parsimonious because the fraction of dose transformed into the metabolite is
   
 155 driven by the two absorption rate constants. The last model, on the right end of Figure 2, includes
   
 a dose apportionment independent of the rate constant values ( $K_{ap}$  and  $K_{am}$ ) with a fraction  $F_p$ 
  
 of the dose leading to the parent and a fraction  $1-F_p$  leading to the metabolite prior to reach the
   
 plasma. Such presystemic formation of an interconversion metabolite is mentioned in the extensive
   
 review on reversible metabolic systems from Cheng and Jusko (18). For identifiability purposes,
   
 160 the fraction of dose available after absorption ( $f$ ) was set to 1.

Also, for all these models, it is noteworthy that all PK parameters cannot be estimated in the
   
 present study, since only an oral administration of the parent drug was performed. Estimating all
   
 PK parameters requires that both the parent drug and the metabolite be given by the intravenous
   
 route in addition to the oral administration of the parent compound (18). It results that only
   
 165 "apparent" parameters can be estimated. The following parameters were identified for the last
   
 model:  $V_p/F_p$ ,  $V_m/(1-F_p)$ ,  $E_1 = k_{po} + k_{pm}$ ,  $E_2 = k_{mo} + k_{mp}$ ,  $k_{pm}F_p/(1-F_p)$  and  $k_{mp}(1-F_p)/F_p$ . An

alternative parameterization is given in Appendix. As our objective was here to assess the impact of genetic covariates on specific clearances ( $CL_{mo}$  for *CYP2D6* and  $CL_{po}$  for *CYP2C19*), it was necessary to make an assumption on the parameters to estimate all clearances separately (and not  
170 global clearances divided by the corresponding volume). Thus, we chose to set  $V_m$  equal to  $V_p$ . In this respect,  $F_p$ ,  $V_p$  and the clearance estimates presented here are tagged by a \* as a reminder of their reliance on the assumption made on volumes. All drug transfers between compartments were modelled as linear processes.

Population parameter estimation was performed in parallel with the FOCE-I and SAEM  
175 algorithms implemented in the NONMEM and MONOLIX softwares, respectively. The first algorithm performs an approximation of the model with a first-order linearisation around the individual predictions of the random effects. In contrast, the second algorithm is a stochastic version of the well-known Expectation-Maximization algorithm where the individual random effects are the missing variables. In the expectation step, the individual parameters are simulated using a  
180 Monte-Carlo Markov Chain approach and then used to compute a stochastic approximation of the conditional expectation of the complete log-likelihood which is the log-likelihood of the complete data, i.e the observations and the imputed individual parameter estimates at the current iteration of the SAEM algorithm. Then, the complete log-likelihood is maximized to obtain the updated estimates of the population parameters. In NONMEM, the convergence of the FOCE-I algorithm is  
185 achieved when all parameters have the required number of significant digits, while in Expectation Maximization-like methods the definition of convergence is usually left to the user discretion. In MONOLIX additionally to the visual inspection of convergence graphics, stopping rules are available which are based on the absence of decrease of the complete log-likelihood sequence during the stochastic step and small variability between subsequent population parameter estimates and  
190 estimates of the complete log-likelihood during the cooling step.

In both NONMEM and MONOLIX, the Fisher Information Matrix and the loglikelihood of the model were obtained by linearization of the model around the predictions of the individual parameters. In NONMEM, we used the OPTION UNCONDITIONAL in the covariance step to overcome the convergence issue as well as the OPTION MATRIX=R and MATRIX=S when

195 needed.

The models were encoded through ODE as well as using the corresponding CF solution derived using the Laplace transform approach (19, 20) (see appendix). For the models encoded with ODE system, data were fitted using the ADVAN5 routine in the NONMEM software version 7.2 and MLXTRAN with the STIFF option in MONOLIX version 2.4. For the models with a dose  
200 apportionment, we used the ADVAN6 routine because of an issue in the ADVAN5 routine to be fixed in the next version of NONMEM. For the models encoded in CF solution, data were fitted using the PRED routine in the NONMEM software version 7.2 and the model building function of MONOLIX version 2.4.

In NONMEM, the number of digits required for convergence (SIG) was set to its default value  
205 of 3 for ADVAN5 and to 3 or 2 for ADVAN6 with a fortran 95 compiler. With ADVAN6, we set the number of significant digits for the predicted values (TOL) to 6 and the number of significant digits for the objective function (SIGL) to 6 in the estimation step and TOL=6 with SIGL=6 in the covariance step, following guidance from (6); with ADVAN5 the TOL option is not required. In MONOLIX, the algorithm settings were left to the default values; the maximal numbers of  
210 stochastic (K1) and cooling (K2) iterations were set to 500 and 200 respectively, with use of automatic stopping rules and only one markov chain (nmc).

The structural model was determined on the data collected at W4 only and all the systems were considered at steady state with a 24 hours dosing interval. We used an exponential model for the between subject variability to ensure positivity of the individual PK parameters and a  
215 logit model to force  $0 \leq F_p \leq 1$ . Along the structural model selection, random effects for all parameters but  $f$  were assumed to follow a normal distribution with a diagonal variance matrix. A combined error model with an additive component  $a$  and multiplicative coefficient  $b$  was used for the parent drug and the metabolite. Model selection was performed using the Bayesian information  
220 criteria (21):  $BIC = -2L + P_{pop} \log(N)$ , where  $L$  is the loglikelihood of the model,  $P_{pop}$  is the number of population parameters which includes the fixed effects, and the variance components and  $N$  the number of subjects. BIC allows to compare both nested and non nested models such as those including  $F_p$  or not. In order to compare the NONMEM and MONOLIX output, we

retrieved  $-2L$  for each model by adding  $n_{tot} \times \log(2\pi)$  to the objective function estimate,  $n_{tot}$  being the total number of observations. Also in the present work we used  $N$  rather than  $n_{tot}$  in the BIC penalizing term, as the observations are dependent within each subject (22, 23).

Once the structural model was selected, parsimonious error models (additive and proportional) were tested using the likelihood ratio test (LRT). To capture clearance and volume correlations due to bioavailability variation, between-subject variance was estimated on  $f$ . Next, between-subject variance ( $\omega^2$ ) nullity was tested using a LRT with, as a reference distribution, a mixture of a  $\chi^2$  distribution with 0 degree of freedom and  $\chi^2$  distribution with 1 degree of freedom (24). Finally, data at W8 were added to the data set and forward inclusion of within-subject variances ( $\gamma^2$ ) was performed on parameters with non-null between-subject variance.

### ***Covariate model***

A linear dose effect was systematically investigated on  $f$  and  $F_p$  parameters using the Wald test. The dose was analyzed as a continuous covariate with 10 mg as the reference dose, so that  $f$  and  $F_p$  of subject  $i$  at occasion  $k$  were predicted as described in equations (1) and (2).

$$f_{ik} = f e^{\beta_{f,D}(D_i-10)} \quad (1)$$

$$F_{p,ik} = \frac{\frac{F_p}{1-F_p} e^{\beta_{F_p,D}(D_i-10)}}{1 + \frac{F_p}{1-F_p} e^{\beta_{F_p,D}(D_i-10)}} \quad (2)$$

Also, linear effects of the *CYP2D6* and *CYP2C19* polymorphisms were investigated following a forward selection based on the Wald test with a significance threshold at 5%. Both genetic covariates were analyzed by means of a phenotypic binary categorization; poor metabolizer (PM) *versus* the reference class the extensive metabolizer (EM), so that the parameter  $\theta$  of subject  $i$  at occasion  $k$  was predicted as described in equation (3) where  $\beta_{\theta,CYP^*}$  was non-null for patients CYP\* EM and 0 otherwise.

$$\theta_{ik} = \theta e^{\beta_{\theta,CYP^*}} \quad (3)$$

The classification was performed as follows: carriers of two rare allele were classified as PM (25).

245 In order to correct the inflation of the Wald type I error shown to occur on unevenly distributed genotypes (14), final p-values were assessed using permutations (15). The null hypothesis of the permutation test is that the mean value of the parameter  $\theta$  would be the same whatever the *CYP2D6* and *CYP2C19* status while the alternative is that the mean value would be different between the poor and extensive metabolizers. More specifically, 1000 data sets were generated  
250 by permuting the rows of the covariate matrix from the original data set. For each covariate, one Wald statistic,  $W^{obs}$ , was estimated from the original data and one Wald statistic,  $W^{perm}$ , was estimated from each of the 1000 data sets. Thus, we obtained  $j=1,\dots,1000$   $W^{perm_j}$ . The permutation p-value was the proportion :  $(\text{card}(W^{perm_j} \geq W^{obs})+1)/(1000+1)$ . As the patients were sampled on two occasions, we also computed a metric representing the genetic component  
255 of variability  $R_{GC} = \max\left(0, 1 - \frac{\gamma^2}{\omega^2}\right) \times 100$  (26), for each model parameter with non-null within-subject variance. This component gets closer to 100% when the between-subject variance for the parameter under study is larger than its within-subject variance, so that the variability for this parameter is more likely to be explained by a genetic covariate.

As mentioned previously, the covariate analysis was performed with the assumption  $V_m = V_p$ .  
260 As the parameter estimates are dependent on this assumption, we have also derived apparent parameters that are independent of any assumption made:  $V_p/F_p$ ,  $V_m/(1 - F_p)$ ,  $CL_{ptot}/F_p$ ,  $CL_{mtot}/(1 - F_p)$ ,  $CL_{pm}/V_m$  and  $CL_{mp}/V_p$  (see appendix). The fixed effects and between-subject standard deviation of these apparent parameters were derived by simulation using our final parameter estimates.

## 265 ***Model evaluation***

An internal model evaluation was performed on both occasions as well as an external model evaluation which only considered one occasion.

For the internal model evaluation before the addition of the genetic effect, we performed visual predictive check plots where the 90% confidence intervals around the 5<sup>th</sup>, 50<sup>th</sup> and 95<sup>th</sup>  
270 prediction percentiles from 250 simulated data sets were overlaid to the 5<sup>th</sup>, 50<sup>th</sup> and 95<sup>th</sup> percentiles of the observed data binned using the theoretical sampling times (27). Then after

the addition of the genetic effect, we computed the normalized prediction distribution errors (npde), i.e. the observation percentiles within the empirical distribution obtained from the model simulations, decorrelated and normalized using the inverse function of the normal cumulative  
275 density function (28).

For the external evaluation of the model after the addition of the genetic effect, we computed the npde and performed a visual predictive check plots where the 5<sup>th</sup>, 50<sup>th</sup> and 95<sup>th</sup> predicted percentiles from 250 simulated data sets were overlaid to the observed 5<sup>th</sup>, 50<sup>th</sup> and 95<sup>th</sup> percentiles of the observed data binned using the theoretical sampling times (27).

280 For the internal and the external model evaluation based on npde, 1000 data sets were simulated and we used the R npde package (29) for the calculations.

## RESULTS

### *Data*

The phase II study data set combining the observed profiles at both occasions contained 101  
285 patients. Thirty five patients had a dose of 5 mg, 31 a dose of 10 mg and 35 a dose of 20 mg. The average [range] age in the population was 40 years [22-64], the average weight 69.0 kg [43.6-120.0] and 53.5% were men. Among the 101 patients: 12 patients were classified as *CYP2D6* PM and 2 were classified as *CYP2C19* PM. Four of the *CYP2D6* PM patients received a dose of 5 mg, 6 received a dose of 10 mg and 2 received a dose of 20 mg. The two *CYP2C19* PM patients received  
290 a dose of 5 mg and 20 mg, respectively. Genotype information was not available in 2 patients.

On W4, 355 and 358 concentrations were measured for the parent drug and the metabolite respectively in 97 patients, 81 of whom had a complete profile of four samples for both compounds. On W8, 271 and 268 concentrations were measured for the parent drug and the metabolite respectively in 71 patients, 51 of whom had a complete profile for both compounds. Sixty-seven  
295 patients had concentration-time profiles at both W4 and W8. Only 8 concentrations out of 1252 (less than 1%) were below the limit of quantification and were discarded from the analysis.

Figure 2 displays the observed concentrations for the parent drug and the metabolite on both

normal and semi-log scales *versus* the time at W4 and W8, revealing a much larger accumulation for the metabolite than for the parent drug.

300 In the external evaluation data set, the average age was 28 years [18-45], the average weight 72.5 kg [63.0-99.3] and all patients were men. Eight patients had a dose of 10 mg, 8 a dose of 20 mg and 7 a dose of 30 mg. After two weeks of repeated oral doses, 203 concentrations were measured for the parent drug and the metabolite in 23 healthy volunteers, 20 of whom had a complete profile of ten samples for both compounds. No concentrations were below the limit of quantification.

### 305 ***Structural and variability models***

Using FOCE-I in NONMEM and SAEM in MONOLIX, convergence was achieved for all models with both coding conditions (ODE or CF). However with FOCE-I in NONMEM, standard error estimates could only be obtained for the models with dose apportionment in ODE.

Table I reports the BIC along with the error model variance component estimates as well as  
310 the computation time for the four structural models investigated plus the model with  $K_{ap} = K_{am}$ , using both software and codings on data at W4. Confirming pre-existent knowledge, the addition of the back-transformation mechanism greatly improved the model with a 100 units drop in BIC. The addition of a first-pass effect led to a 40 units decrease in BIC further lowered with the inclusion of an additional  $F_p$  term for the dose apportionment. Estimates of error model components were  
315 quite close across algorithms and coding with the exception of the additive coefficient for the parent drug. Yet, the relative standard error (RSE) obtained with FOCE-I in NONMEM and/or MONOLIX for this parameter was always very large (data not shown). For the most complex model, computation times dramatically decreased when using CF instead of ODE irrespective of the software (53.8 h to 22.2 min using NONMEM and 2.42 h to 0.6 min using MONOLIX).

320 The fixed effect estimates were similar when using ODE or CF for the same model and estimation algorithm, as shown in Table II. The median and maximal relative difference on clearances were respectively 0 and 47% with FOCE-I and 3 and 45% with SAEM in MONOLIX. For the two models without first-pass effect, the FOCE-I estimates were always included in the confidence intervals of the SAEM estimates. Whereas for the model with first-pass effect but no

325 dose apportionment, the FOCE-I estimates for the volumes and all clearance but  $CL_{mp}^*$  did not fall within the confidence intervals of the SAEM estimates. For the model with dose apportionment and similar absorption rates, the confidence intervals of the FOCE-I estimates in ODE always included the FOCE-I estimates in CF and overlapped with the confidence intervals of the SAEM estimates. However with FOCE-I, the clearance of the parent by other pathways ( $CL_{po}^*$ ) was 330 greater than the clearance of transformation of the parent into the metabolite ( $CL_{pm}^*$ ) while with SAEM  $CL_{po}^* < CL_{pm}^*$ . Also with FOCE-I, the clearance of the metabolite by other pathways ( $CL_{mo}^*$ ) was similar to the clearance of transformation of the metabolite into the parent ( $CL_{mp}^*$ ) while with SAEM  $CL_{mo}^* > CL_{mp}^*$ .

Table III displays the between-subject standard deviation estimates of the four structural 335 models as well as the model with similar absorption rates. The between-subject standard deviation estimates showed greater discrepancies using ODE or CF for the same model and estimation algorithm. Indeed, the median and maximal relative difference on clearance standard deviation estimates were respectively 0 and 150% with FOCE-I in NONMEM and 1.8 and 44% with SAEM in MONOLIX. As for the similarity based on the confidence intervals of the FOCE-I and/or SAEM 340 estimates, the pattern was similar to that for the fixed effect. Of note with FOCE-I,  $\omega_{CL_{pm}^*}$  and  $\omega_{CL_{mp}^*}$  estimates were very close to zero, while zero was either included in, or very close to the boundaries of the corresponding confidence intervals of the corresponding SAEM estimates.

The model selection proceeded similarly using either FOCE-I in NONMEM or SAEM in MONOLIX and ODE or CF, with the selected model including a back-transformation mechanism 345 and a first-pass effect with a  $F_p$  parameter for the dose apportionment. Both absorption/formation rate constants were difficult to estimate across models due to the combination of a 10 times ratio with the elimination rates and limited plasma data early after dose administration. Thus, we investigated a reduced model with similar absorption/formation rate constants for the parent drug and the metabolite. The BIC decreased by 30 units so that we kept this model for subsequent 350 analyses. The RSE on the absorption rate constant in this model were about 15% with FOCE-I in NONMEM in ODE and 46 and 54% with SAEM in ODE and CF, respectively. Given the shorter computation time and the possibility to obtain standard error estimates, the MONOLIX software

with the model encoded in closed form solution was used in the following.

A proportional and a combined error model were selected for the parent drug and its metabolite, respectively, with estimates for the multiplicative component about 30% and 6%. Of note in the model including the  $f$  parameter, the BIC was reduced by 100 units using a diagonal-covariance matrix for the random effects compared to a full-matrix where the smallest and largest correlation estimates were -0.09 and 0.71, respectively. Then, estimation of between-subject variance was found to improve BIC for all parameters except the fraction of dose that escaped first-pass effect ( $F_p^*$ ),  $CL_{mp}^*$  and  $CL_{pm}^*$ . Once included the data at W8, the absorption constant rate had to be fixed to its estimate on data at W4 for stability purposes. Only the within-subject variance of the  $CL_{po}^*$  was significantly different from 0.

### ***Covariate model***

It appears that the  $f^*$  and  $F_p^*$  were 10 and 22% higher for a 5 mg dose and 19 and 33% lower for a 20 mg dose respectively (both p-values <  $10^{-3}$ ). The population parameter estimates of the basic model not including the genetic covariate and their relative standard error (RSE) are given in Table IV, for the 101 patients of the phase II study. Figure 4 represents the visual predictive check (VPC) plots obtained for each compound at both occasions and for the three doses. The predictions from the model described adequately the observed high and median concentration profiles of both molecules for the three doses. However, the model seems to predict less well the low concentration-time profiles, with a systematic overprediction at time 1h for the parent together with an underprediction of the ensuing times for the 5 mg dose on both occasions and the 10 mg dose at W8. For the metabolite, the VPC plots indicate a misfit for the low concentration-time profiles for the 10 mg dose at W4. It is noteworthy though that some of these misfits might be explained by some atypical individual profiles (see figures 3c and 3d), which drive the lower observed percentile estimates at doses 5 and 10 mg.

The genetic effect analysis indicated that  $CL_{mo}^*$  was decreased by 34% (p-value=0.015, Wald test by permutation) in *CYP2D6* PM patients. The population parameters of the model including the genetic covariate and their RSE are given in Table IV, for the 99 patients with available

380 genotyping for the *CYP2D6* polymorphisms. Based on these estimates for a *CYP2D6* EM patients at a dose of 10 mg, the following estimates could be derived for the apparent parameters (with between-subject, and when applicable, within subject standard deviation in brackets)  $V_p/F_p=22.34$  (0.42) L,  $V_m/(1-F_p)=145.27$  (0.42) L,  $CL_{ptot}/F_p=3.19$  (1.58 and 0.83) L.h<sup>-1</sup>,  $CL_{mtot}/(1-F_p)=4.40$  (0.65) L.h<sup>-1</sup>,  $CL_{pm}/V_m=0.11$  (0.28) h<sup>-1</sup> and  $CL_{mp}/V_p=0.004$  (0.28) h<sup>-1</sup>. Figure 5 represents the 385 distribution of the concentrations at each dose level between PM and EM. The rise in metabolite concentration levels in *CYP2D6* poor metabolizers compared to extensive metabolizers appeared clearly in all dose groups while for the parent drug, the impact was only noticeable at the 20 mg dose. The between-subject standard deviation for  $CL_{mo}^*$  was only slightly decreased with the incorporation of the covariate. However, it is noteworthy that there were only 12 *CYP2D6* PM 390 patients in this study. Following Özdemir definition (26),  $R_{GC}$  was computed only for  $CL_{po}^*$  because it was the only parameter with non-null within-subject variance. In this study, the  $R_{GC}$  for  $CL_{po}^*$  was equal to 0 as  $\gamma_{CL_{po}^*}^2$  was superior to  $\omega_{CL_{po}^*}^2$  and indeed no genetic effect was found on this parameter. No effect of the *CYP2C19* polymorphisms was found, probably due to the small number of PM.

395 Figure 6 displays the npde from the model including the genetic covariate *versus* time for the parent drug and the metabolite on both occasions in the original data set. For the parent, the npde at 3, 6 and 24h were evenly distributed around 0 with the colored area formed by the 90% interval almost confounded with the dashed lines that represent the 5<sup>th</sup> and 95<sup>th</sup> percentiles of the normal distribution. Yet at time 1h on both occasions, the npde showed a deviation which was previously 400 observed on the visual predictive check plots and the corresponding global tests p-values given in the output of the npde calculation were below 0.001. The bias at time 1h might be explained by the existence of a few patients with a slower absorption whose S33138 profile is not accurately described by the model. For the metabolite, the npde appeared randomly distributed around 0 and within the required boundaries but the corresponding global tests p-values were also below 405 0.001. Figure 7 and 8 present respectively the npde and a visual predictive check plots from the model including the genetic covariate *versus* time for the parent drug and the metabolite in the external evaluation data set. The npde for the parent drug tended to be below zero, especially in

the first times but remained above the 5<sup>th</sup> percentiles of the normal distribution. Also, the colored area formed by the 90% interval was somewhat narrower than expected and the corresponding global tests p-values were below 0.001. Similarly on the visual predictive check plots, the 5<sup>th</sup> and 95<sup>th</sup> predicted percentiles were respectively lower and higher compared to the observed percentiles, especially for the 95<sup>th</sup> percentiles of the parent drug at the 20 mg dose. Nevertheless the observed and predicted median were satisfactorily close.

In conclusion, the final model provided sensible predictions of the observations despite some difficulties in capturing the lower concentration profiles in patients and an overprediction of the variability in healthy volunteers. Due to these misspecifications, the model was rejected based on the npde global test. However, the heterogeneity in absorption at 1h could be tackled in future analyses using mixture models to account for the diet or other unknown factors and healthy volunteers are known to be a less heterogeneous population than patients. This model, involving back-transformation and first-pass effect, had though to be parsimonious given the study design.

## DISCUSSION

In the present work, we compared four different structural models to describe the concentration-time profiles of a novel antipsychotic and its active metabolite obtained at two occasions. We used the FOCE-I algorithm in NONMEM and the SAEM algorithm in MONOLIX to fit the data using models encoded both in ODE and CF solutions. With the final selected model, we investigated the effect of the metabolizer status as defined by *CYP2D6* and *CYP2C19* polymorphisms on the PK of the parent drug and its metabolite.

The PK of both compounds was reasonably well described by a model including a back-transformation mechanism and a first-pass effect with an additional term for the dose apportionment. Cheng and Jusko (18) defined the acetylation of the metabolite to form back its acetylated parent as a known process for numerous amines, in their extensive review on reversible metabolic systems. They also mentioned the occurrence of presystemic formation of an interconversion metabolite and the consequences in determining the rates and extents of drug absorption and presystemic formation of an interconversion metabolite. In addition, this

reference work lists several formulas to derive PK parameters for compounds with interconversion  
metabolite(s), based on AUC ratio and/or numerical deconvolution after a separate analysis of the  
parent and/or metabolite profiles. Here, we chose to model both compounds jointly, to provide  
PK parameter fixed effects and variance estimates in patients. In the present study, the back-  
transformation process provided a mechanism-based explanation for the long terminal plasma  
half-life observed for the parent drug with reduced accumulation at steady-state. Actually, the  
terminal plasma half-lives derived from our model for the parent drug and metabolite were similar,  
yet the parent drug showed an effective half-life of 8.5 h i.e. 4 times faster than that of the  
metabolite (32.7 h) (30). The first-pass effect, on the other hand, allowed to capture the early  
bump observed in the metabolite data. Auclair et al. also showed that adding a first-pass effect  
in their model allowed to fit metabolite concentrations that appeared quicker or at the same time  
as the parent drug (31). Such a first-pass effect through amidases in the gut and the liver has  
already been observed in more dramatic proportions for the experimental anti-convulsant related  
to lidocaine, D2624 (32). In our final model, the rate of appearance of the metabolite,  $K_{am}$  was  
set to the absorption rate of the parent drug  $K_{ap}$ . We explain this finding by the fact that the  
absorption rate of the parent drug would be rate limiting due to the very quick formation of the  
metabolite. Duffull et al. also reported this phenomenon for ivabradine and its metabolite in (33).

Thorough mathematical investigations were required to identify the apparent PK parameters  
which are presented here for the final and more complex model (first-pass effect with back-  
transformation of the metabolite) in the appendix of the article. Yet, interpretation of apparent PK  
parameters is not always straightforward, and they may not allow proper covariate analysis. For  
instance, the effect of *CYP2D6* was expected on  $CL_{mo}$  only, given prior knowledge, with no impact  
on  $CL_{mp}$  so using the apparent parameter  $CL_{mtot}/(1 - F_p)$  would not have been appropriate. For  
this reason, we have decided to make an assumption on volumes in order to be able to estimate all  
clearances separately. By convenience, we chose to set the volumes equal as this allowed estimation  
of between and within-subject variability on parent and metabolite volumes. This assumption  
was judged reasonable since the ratio of 1 is in the range of volumes ratios estimated from the  
microdose study and gives estimates for the bioavailability and the percentage of dose undergoing

back-transformation close to those obtained from the microdose study where clearances of all processes were identifiable. The microdose study gave a median [range] volume of distribution of 465 78 L [60-287] for the parent and 48 L [30-129] for the metabolite, with a volume ratio of 2.4 [0.5-6]. It is obvious that  $F_p$ ,  $V_p$  and clearance estimates depend on the assumption we made on the ratio of volumes but setting the volumes ratio to 2.4 in the final model did not markedly impact the results of the analysis apart a significant higher estimate for the percentage of dose undergoing back-transformation (10 % instead of 5 %) which is less in agreement with the microdose study 470 results.

In silico measures of  $\log P=2.29$  and  $2.36$ ,  $\log D$  (pH7.4)= $1.24$  and  $1.32$  and  $pK_{a1}=8.46$  and  $8.46$  (tertiary amine) between respectively the parent and the metabolite were similar with the exception of  $pK_{a2}=12.43$  (amide) and  $4.73$  (primary amine). This information neither supported nor infirmed the assumption on the ratio of volumes. Moreover, the volume of distribution also 475 depends on the compound affinity for transporters or tissues as well as its binding ability to plasma proteins. In the present analysis, models with saturable elimination were not investigated as neither the prior knowledge on the compounds nor the goodness of fit plots suggested the existence of such a process. Also, models with a central and peripheral compartment for the parent and metabolite were not evaluated because of the sparse study design which would have 480 not enabled robust estimation.

Here, two estimation algorithms implemented in two softwares were used for data analysis. As regulatory authorities encourage the use of new estimation algorithms, this work addresses a current and relevant issue with a comparison of both software on such a complex model and using both codings. The SAEM algorithm has been recently implemented in NONMEM version 485 7. Yet, we chose its implementation in MONOLIX because it has been thoroughly evaluated compared to the more recent NONMEM one. Both algorithms led to the selection of the same structural model whatever the coding approach. However, substantial differences between the standard deviation estimates were observed across codings for the same model and same estimation algorithm. An extensive comparison of both softwares performances has been already performed 490 and is currently available on the MONOLIX website (<http://software.monolix.org/sdoms/>

software/index.php?/evaluation.html). However, the models investigated were less advanced and all considered only one response. In the present work, using two estimation algorithms was a complementary investigation and a proper comparison would require simulations from known parameters and models. Taking these limitations into account, some differences in parameter estimates were observed. Among the two software, the absorption rate estimates were those that differed the most, but they were also the most difficult to evaluate. The lack of sampling times early after dose administration led to poorly estimable absorption rate constants. Yet, we chose not to fix these parameters for the structural model building because this was the first modelling of S33138 and S35424 pharmacokinetics performed in patients and this population can greatly differ from healthy volunteers. Also, we were comforted in our decision by the consistency in the BIC and other parameter estimates. Difficulties were met to obtain SEs with FOCE-I in NONMEM despite using several sets of different initial conditions, however we did not systematically investigate initial conditions (this could be done using hypercube sampling in the multi-dimensional space of parameter). Non-parametric bootstrap can be performed to obtain an empirical distribution of the parameter uncertainty but in the present work we have performed permutation based Wald tests to correct for the departure from asymptotic conditions. Both procedures are computationally intensive and are facilitated by the use of closed form solutions which provides an important gain of time. While NONMEM easily handles steady state concentrations with model encoded in ODE, MLXTRAN in MONOLIX version 2.4 requires the user to add dummy lines of dose to mimic the path to steady state. The difference in computation time using this coding approach would thus increase with the number of subjects and the time to reach steady state.

*CYP2D6* is an important catalyst of the oxidation of various antipsychotic agents: chlorpromazine, thioridazine, risperidone and haloperidol (34). Recently, significantly higher risperidone and 9-hydroxyrisperidone (its active metabolite) plasma concentrations have been observed in Korean *CYP2D6* PM (35). Here, both the metabolite and the parent drug showed a higher plasma exposure (AUC) in *CYP2D6* PM patients compared to EM patients. This indicates that the back-transformation of the metabolite to the parent affects the disposition of the parent drug although concerning only 6% of the dose (30). Hamrén et al. have also described the

impact of metabolite decreased elimination on parent drug concentrations in the presence of a  
520 reversible metabolism; in patients with impaired renal function, the decreased renal elimination of  
the tesaglitazar metabolite (acyl glucuronide) causes an increase of the metabolite in plasma, which  
leads to increased amounts of metabolite undergoing back-transformation and subsequently an  
accumulation of tesaglitazar (17). In this respect, despite some limitations of the model (i.e. its  
apparent difficulty in capturing the lower concentration profiles in patients), the present work opens  
525 some perspectives for the ongoing development of the antipsychotic. The occurrence of *CYP2D6*  
PM is higher in Caucasians (5-10%) than in East Asians (about 1%) (36) and the *CYP2D6*  
activity is lower in Chinese EM compared to Caucasians (36) due to the *CYP2D6\*10* allele. Thus,  
additional investigations should be useful to assess the impact of *CYP2D6* polymorphisms in  
populations other than Caucasians. As the model does not correctly predict the variability in  
530 healthy volunteers, it may not be used for comparison of Caucasian and Asian healthy volunteers.  
However, it may be used as a model for Caucasian patients. Indeed, despite the lack of intravenous  
data in patients and identifiability problems, the present model give sensible predictions of the  
concentrations of the parent drug and the metabolite in patients and of the effect of CYP2D6 on  
plasma exposure.

## 535 CONCLUSION

Using both algorithms and coding, we developed a complex joint pharmacokinetic model of interest  
for further developments of an antipsychotic and its metabolite. This model enabled us to evidence  
the *CYP2D6* polymorphisms influence on the elimination of the active metabolite and adequately  
predict its impact on the parent drug levels through a back-transformation mechanism.

## 540 ACKNOWLEDGMENTS

The authors would like to thank Pr. N. Holford for his clever inputs on the choice of the parameter's  
notation to facilitate the understanding of the different structural models. We would also like to  
thank the MONOLIX development team for making the MLXTRAN tool available for this work.

During this work, Julie Bertrand was supported by a grant from the Institut de Recherches  
545 Internationales Servier (France).

## References

1. Shargel L, Wu-Pong S, Yu A. Applied Biopharmaceutics & Pharmacokinetics. 5th ed. USA: McGraw-Hill Medical; 2005.
2. Younis IR, Malone S, Friedman HS, Schaaf LJ, Petros WP. Enterohepatic recirculation model  
550 of irinotecan (CPT-11) and metabolite pharmacokinetics in patients with glioma. *Cancer Chemother Pharmacol.* 2009;63:517–524.
3. Panhard X, Goujard C, Legrand M, Taburet AM, Diquet B, Mentré F. Population pharmacokinetic analysis for nelfinavir and its metabolite M8 in virologically controlled HIV-infected patients on HAART. *Br J Clin Pharmacol.* 2005;60:390–403.
- 555 4. Feng Y, Pollock BG, Coley K, Marder S, Miller D, Kirshner M, et al. Population pharmacokinetic analysis for risperidone using highly sparse sampling measurements from the CATIE study. *Br J Clin Pharmacol.* 2008;66:629–639.
5. Lindstrom M, Bates D. Nonlinear mixed effects models for repeated measures data. *Biometrics.* 1990;46:673–687.
- 560 6. Beal S, Sheiner L, Boeckmann A, Bauer R. NONMEM User's Guides (1989-2009). Ellicott City, MD, USA; 2009.
7. Girard P, Mentré F. A comparison of estimation methods in nonlinear mixed effects models using a blind analysis. Pamplona, Spain: 14th Population Approach Group in Europe; 2005. Available from: <http://www.page-meeting.org/page/page2005/PAGE2005008.pdf>.
- 565 8. Bertrand J, Comets E, Mentré F. Comparison of model-based tests and selection strategies to detect genetic polymorphisms influencing pharmacokinetic parameters. *J Biopharm Stat.* 2008;18:1084–102.

9. Kuhn E, Lavielle M. Maximum likelihood estimation in nonlinear mixed effects models. *Comput Stat Data Anal.* 2005;49:1020–38.
- 570 10. Lavielle M. MONOLIX (MOdèles NON LInéaires à effets miXtes). Orsay, France; 2008. <http://software.monolix.org/index.php>.
11. Bauer RJ. S-ADAPT/MCPEM User's Guide Version 1.56. Los Angeles, CA, USA; 2008.
12. Millan MJ, Loiseau F, Dekeyne A, Gobert A, Flik G, Cremers TI, et al. S33138 (N-[4-[2-[(3aS,9bR)-8-cyano-1,3a,4,9b-tetrahydro[1] benzopyrano[3,4-c]pyrrol-2(3H)-  
575 yl)-ethyl]phenyl-acetamide), a preferential dopamine D3 versus D2 receptor antagonist and potential antipsychotic agent: III. Actions in models of therapeutic activity and induction of side effects. *J Pharmacol Exp Ther.* 2008;324:1212–1226.
13. Zhou S, Liu J, Chowbay B. Polymorphism of human cytochrome P450 enzymes and its clinical impact. *Drug Metab Rev.* 2009;41:89–295.
- 580 14. Bertrand J, Comets E, Laffont C, Chenel M, Mentré F. Pharmacogenetics and population pharmacokinetics: impact of the design on three tests using the SAEM algorithm. *J Pharmacokinet Pharmacodyn.* 2009;36:317–339.
15. Manly B. Randomization, Bootstrap and Monte Carlo Methods in Biology. 2nd ed. London: Chapman & Hall; 1998.
- 585 16. Brendel K, Dartois C, Comets E, Lemenuel-Diot A, Laveille C, Tranchand B, et al. Are population pharmacokinetic and/or pharmacodynamic models adequately evaluated? A survey of the literature from 2002 to 2004. *Clin Pharmacokinet.* 2007;46:221–234.
17. Hamrén B, Ericsson H, Samuelsson O, Karlsson M. Mechanistic modelling of tesaglitazar pharmacokinetic data in subjects with various degrees of renal function—evidence of  
590 interconversion. *Br J Clin Pharmacol.* 2008;65:855–63.
18. Cheng H, Jusko W. Pharmacokinetics of reversible metabolic systems. *Biopharm Drug Dispos.* 1993;14:721–66.

19. Gibaldi M, Perrier D. Pharmacokinetics. 2nd ed. New York: Marcel Dekker; 1982.
20. Vaughan D, Mallard D, Trainor A, Mitchard M. General Pharmacokinetic Equations for  
595 Linear Mammillary Models with Drug Absorption into Peripheral Compartments. *Europ J  
Clin Pharmacol.* 1975;8:141–8.
21. Schwartz G. Estimating the dimension of a model. *Ann Stat.* 1978;6:461–464.
22. Faes C, Molenberghs G, Aerts M, Verbeke G, Kenward MG. The Effective Sample Size and an  
Alternative Small-Sample Degrees-of-Freedom Method. *American Statistician.* 2009;63:389–  
600 399.
23. Visser I, Ray S, Jang W, Berger J. Effective Sample Size and the Bayes Factor. Research  
Triangle Park, NC: Workshop on Latent Variable Modeling in Social Sciences, SAMSI; 2006.
24. Stram DO, Lee JW. Variance components testing in the longitudinal mixed effects model.  
*Biometrics.* 1994;50(4):1171–1177. Available from: <http://www.jstor.org/stable/2533455>.
- 605 25. Chou W, Yan F, Robbins-Weilert D, Ryder T, Liu W, Perbost C, et al. Comparison of  
two CYP2D6 genotyping methods and assessment of genotype-phenotype relationships. *Clin  
Chem.* 2003;49:542–51.
26. Ozdemir V, Kalow W, Tang B, Paterson A, Walker S, Endrenyi L, et al. Evaluation of the  
genetic component of variability in CYP3A4 activity: a repeated drug administration method.  
610 *Pharmacogenetics.* 2000;10:373–88.
27. Karlsson M, Holford N. A Tutorial on Visual Predictive Checks. Marseille, France: 17th  
Population Approach Group in Europe; 2008. Available from: [http://www.page-meeting.  
org/pdf/\\_assets/8694-Karlsson\\\_Holford\\\_VPC\\\_Tutorial\\\_hires.pdf](http://www.page-meeting.org/pdf/_assets/8694-Karlsson\_Holford\_VPC\_Tutorial\_hires.pdf).
28. Brendel K, Comets E, Laffont C, Mentré F. Evaluation of different tests based on observations  
615 for external model evaluation of population analyses. *J Pharmacokinet Pharmacodyn.*  
2010;37:49–65.

29. Comets E, Brendel K, Mentré F. Computing normalised prediction distribution errors to evaluate nonlinear mixed-effect models: the npde add-on package for R. *Comput Methods Programs Biomed.* 2008;90:154–166.
- 620 30. Rowland M, Tozer T. *Clinical pharmacokinetics. Concepts and Applications.* 3rd ed. USA: Lippincot Williams & Wilkins; 1995.
31. Chou W, Yan F, Robbins-Weilert D, Ryder T, Liu W, Perbost C, et al. Comparison of two CYP2D6 genotyping methods and assessment of genotype-phenotype relationships. *Clin Chem.* 2003;49:542–51.
- 625 32. Martin S, Bishop F, Kerr B, Moor M, Moore M, Sheffels P, et al. Pharmacokinetics and metabolism of the novel anticonvulsant agent N-(2,6-dimethylphenyl)-5-methyl-3-isoxazolecarboxamide (D2624) in rats and humans. *Drug Metab Dispos.* 1997;25:40–6.
33. Duffull S, Chabaud S, Nony P, Laveille C, Girard P, Aarons L. A pharmacokinetic simulation model for ivabradine in healthy volunteers. *Eur J Pharm Sci.* 2000;10:285–94.
- 630 34. Murray M. Role of CYP pharmacogenetics and drug-drug interactions in the efficacy and safety of atypical and other antipsychotic agents. *J Pharm Pharmacol.* 2006;58:871–85.
35. Kang R, Jung S, Kim K, Lee D, Cho H, Jung B, et al. Effects of CYP2D6 and CYP3A5 genotypes on the plasma concentrations of risperidone and 9-hydroxyrisperidone in Korean schizophrenic patients. *J Clin Psychopharmacol.* 2009;29:272–7.
- 635 36. Bertilsson L, Lou Y, Du Y, Liu Y, Kuang T, Liao X, et al. Pronounced differences between native Chinese and Swedish populations in the polymorphic hydroxylations of debrisoquin and S-mephenytoin. *Clin Pharmacol Ther.* 1992;51:388–97.

## LEGEND TO FIGURES

**Figure 1.** Chemical structure of the parent drug: S33138 (a) and its active metabolite: S35424  
640 (b).

**Figure 2.** Schematic representation of the four tested structural models.  $f$ =fraction of dose after absorption,  $D$ =the dose,  $F_p$ =fraction of parent reaching systemic circulation after absorption,  $K_{ap}$ =absorption constant for the parent,  $K_{am}$ =absorption constant for the metabolite,  $V_p$ =volume of distribution for the parent,  $V_m$ =volume of distribution for the metabolite,  $CL_{po}$ =clearance of  
645 the parent by other pathways,  $CL_{pm}$ =clearance of the parent into the metabolite,  $CL_{mo}$ =clearance of the metabolite by other pathways,  $CL_{mp}$ =clearance of back-transformation of the metabolite into the parent drug.

**Figure 3.** Spaghetti plot of the observed concentrations of parent drug and metabolite *versus* time collected on two occasions, four and eight weeks after the treatment onset (W4 and W8) on  
650 a normal (a, b) and semi-log scale (c, d). The solid lines represent profiles from patients with a dose of 5 mg, dashed lines profiles from patients with a dose of 10 mg and dotted lines profiles from patients with a dose of 20 mg.

**Figure 4.** Confidence interval visual predictive check plots of the selected structural and variability model including the dose effect, on a semi-log scale. The 90% confidence interval around the 5<sup>th</sup>,  
655 50<sup>th</sup> and 95<sup>th</sup> prediction percentiles from 250 simulated data sets are overlaid on the observed 5<sup>th</sup>, 50<sup>th</sup> and 95<sup>th</sup> percentiles for the parent drug (top) and the metabolite (bottom) at W4 and W8 for a dose of 5 mg (a), 10 mg (b) and 20 mg (c).

**Figure 5.** Boxplots of the parent drug (a) and metabolite (b) concentrations in the study, at the three dose levels. The 10<sup>th</sup> percentile corresponds to the lower whisker, the 25<sup>th</sup> percentile to  
660 the lower hinge, the median to the thick bar, the 75<sup>th</sup> percentile to the upper hinge and the 90<sup>th</sup> percentile to the upper whisker.

**Figure 6.** Normalized prediction distribution errors *versus* time from the final covariate model using the model building data set for the parent drug (top) and the metabolite (bottom) at W4 and W8. The corresponding 90% interval and the median are overlaid on the plot, and the dashed  
665 lines represent the 90% interval and median of the normal distribution.

**Figure 7.** Normalized prediction distribution errors *versus* time from the final covariate model using the external evaluation data set for the parent drug (top) and the metabolite (bottom). The corresponding 90% interval and the median are overlaid on the plot, and the dashed lines represent the 90% interval and median of the normal distribution.

670 **Figure 8.** Classic visual predictive check plots of the final covariate model using the external evaluation data set for the parent drug (top) and the metabolite (bottom), on a semi-log scale. The plain lines in grey represent the 5<sup>th</sup>, 50<sup>th</sup> and 95<sup>th</sup> predicted percentiles and the dark dots jointed by dashed lines represent the 5<sup>th</sup>, 50<sup>th</sup> and 95<sup>th</sup> observed percentiles for the parent drug (top) and the metabolite (bottom) for a dose of 10 mg (a), 20 mg (b) and 30 mg (c).

Table I. Bayesian Information Criteria (BIC), residual error model coefficient estimates and the computing time for the four structural models and the model with similar absorption rates, encoded in ordinary differential equations (ODE) and closed form (CF) using both the FOCE-I and the SAEM algorithms implemented in NONMEM and MONOLIX respectively, on data at W4

	BIC	$a_p$	$b_p$	$a_m$	$b_m$	time	
Without interconversion	FOCE-I ODE	10 357	5.82	0.35	89.2	0.05 0.31	
	CF	10 368	4.00	0.36	96.4	0.05 0.14	
SAEM	ODE	10 352	27.60	0.30	105.0	0.05 0.98	
	CF	10 359	28.80	0.30	89.2	0.05 0.01	
With interconversion	FOCE-I ODE	10 241	0.34	0.34	76.2	0.05 0.50	
	CF	10 260	1.64	0.35	85.8	0.05 0.16	
Without first-pass effect	SAEM	ODE	10 253	0.06	0.34	74.1	0.06 1.37
	CF	10 245	0.02	0.34	70.0	0.05 0.01	
With first-pass effect	FOCE-I ODE	10 196	2.84	0.34	71.6	0.05 0.60	
	CF	10 206	2.97	0.35	74.9	0.05 0.27	
Without dose apportionment	SAEM	ODE	10 212	0.08	0.34	74.8	0.05 1.40
	CF	10 215	0.37	0.34	75.3	0.05 0.01	
With dose apportionment	FOCE-I ODE	10 186	2.47	0.34	55.90	0.05 53.8	
	CF	10 196	2.44	0.35	53.0	0.05 0.37	
Different absorption rates	SAEM	ODE	10 176	0.57	0.32	58.3	0.05 2.42
	CF	10 196	0.27	0.33	54.0	0.05 0.01	
With dose apportionment	FOCE-I ODE	10 149	3.65	0.31	51.30	0.05 35.4	
	CF	10 166	3.17	0.32	51.20	0.05 0.45	
Similar absorption rates	SAEM	ODE	10 141	-0.01	0.32	57.90	0.05 2.37
	CF	10 152	0.09	0.32	52.20	0.05 0.01	

*a*: additive coefficient in  $\text{nmol.L}^{-1}$

*b*: multiplicative coefficient

time: computing time in hour

Table II. Fixed effect estimates and their RSE (% , in grey) for the four structural models and the model with similar absorption rates, encoded in ordinary differential equations (ODE) and closed form (CF) using both the FOCE-I and the SAEM algorithms implemented in NONMEM and MONOLIX respectively, on data at W4

	$F_p^*$	$K_{ap}$ ( $h^{-1}$ )	$K_{am}$ ( $h^{-1}$ )	$V_p (=V_m)^*$ (L)	$CL_{po}^*$ ( $L \cdot h^{-1}$ )	$CL_{pm}^*$ ( $L \cdot h^{-1}$ )	$CL_{mo}^*$ ( $L \cdot h^{-1}$ )	$CL_{mp}^*$ ( $L \cdot h^{-1}$ )
Without interconversion	FOCE-I ODE	-	-	25.2	NE	NE	NE	NE
	CF	99.0	NE	-	0.19	2.66	0.61	-
SAEM	ODE	-	-	23.0	4	27	0.46	7
	CF	46.7	133	-	0.57	2.06	6	-
With interconversion	FOCE-I ODE	-	-	20.9	NE	NE	NE	NE
	CF	99.0	NE	-	1.37	2.67	0.38	-
Without first-pass effect	SAEM ODE	-	-	20.9	4	22	0.40	11
	CF	65.6	132	-	1.00	2.95	6	9
With first-pass effect	FOCE-I ODE	-	-	20.8	5	21	0.42	10
	CF	101.0	171	-	0.99	2.91	7	9
Without dose apportionment	FOCE-I ODE	-	0.3	17.4	NE	NE	NE	NE
	CF	1.5	NE	-	2.55	1.34	0.18	-
SAEM	ODE	-	0.3	17.3	NE	NE	NE	NE
	CF	1.5	NE	-	2.53	1.31	0.18	-
With dose apportionment	FOCE-I ODE	-	-	20.8	4	24	0.48	8
	CF	5.4	52	-	0.70	2.36	7	15
Different absorption rates	FOCE-I ODE	-	-	20.8	4	20	0.42	10
	CF	11.4	77	-	1.02	2.39	8	12
With dose apportionment	FOCE-I ODE	0.82	1.88	17.0	NE	NE	NE	NE
	CF	1.87	NE	-	2.54	1.21	0.18	-
SAEM	ODE	0.82	2.05	17.0	NE	NE	NE	NE
	CF	1.92	NE	-	2.45	1.24	0.20	-
With dose apportionment	FOCE-I ODE	0.86	5.9	18.4	5	15	0.34	12
	CF	20.2	84	-	1.39	1.76	9	12
Similar absorption rates	FOCE-I ODE	0.83	7.6	18.3	5	15	0.35	12
	CF	22.0	101	-	1.44	1.80	10	12
SAEM	ODE	0.81	-	16.5	10	34	0.18	21
	CF	1.8	40	-	2.58	1.16	66	0.18
With dose apportionment	FOCE-I ODE	0.81	-	16.6	NE	NE	NE	NE
	CF	2.0	NE	-	2.48	1.20	0.19	-
SAEM	ODE	0.87	-	18.9	4	18	0.39	11
	CF	7.5	46	-	1.15	2.06	8	10
With dose apportionment	FOCE-I ODE	0.85	-	19.4	4	23	0.46	8
	CF	9.3	54	-	0.80	2.33	7	14

NE: not estimated

\* Estimates that rely on the assumption that  $V_m = V_p$

Table III. Between subject standard deviation and their RSE (% in grey) for the four structural models and the model with similar absorption rates, encoded in ordinary differential equations (ODE) and closed form (CF) using both the FOCE-I and the SAEM algorithms implemented in NONMEM and MONOLIX respectively, on data at W4

	$\omega F_p^*$	$\omega K_{ap}$	$\omega K_{am}$	$\omega V_p (= \omega V_m)^*$	$\omega C L_{po}^*$	$\omega C L_{pm}^*$	$\omega C L_{mo}^*$	$\omega C L_{mp}^*$
Without interconversion	FOCE-I ODE	-	0.05 NE	-	2.04 NE	0.30 NE	0.51 NE	-
	CF	-	0.06 NE	-	1.70 NE	0.29 NE	0.51 NE	-
SAEM	ODE	-	2.18 47	-	1.46 14	0.30 12	0.44 15	-
	CF	-	1.60 61	-	1.60 13	0.37 18	0.52 12	-
With interconversion	FOCE-I ODE	-	3.35 NE	-	0.95 NE	0.20 NE	0.60 NE	0.05 NE
	CF	-	0.04 NE	-	0.88 NE	0.21 NE	0.60 NE	0.00 NE
Without first-pass effect	SAEM ODE	-	2.66 39	-	1.09 17	0.21 12	0.62 27	0.31 9
	CF	-	2.94 46	-	0.98 12	0.24 13	0.59 22	0.28 9
With first-pass effect	FOCE-I ODE	-	0.01 NE	0.32 NE	0.55 NE	0.02 NE	0.90 NE	0.01 NE
	CF	-	0.01 NE	0.29 NE	0.55 NE	0.05 NE	0.87 NE	0.01 NE
Without dose apportionment	SAEM ODE	-	0.66 70	0.66 57	1.12 12	0.20 13	0.55 30	0.36 9
	CF	-	0.68 96	0.76 78	0.90 14	0.23 12	0.57 28	0.29 9
With dose apportionment	FOCE-I ODE	0.00 NE	0.00 NE	1.37 NE	0.54 NE	0.00 NE	0.91 NE	0.00 NE
	CF	0.00 NE	0.00 NE	1.42 NE	0.54 NE	0.00 NE	0.86 NE	0.00 NE
Different absorption rates	SAEM ODE	0.44 46	2.13 32	1.51 57	0.78 12	0.20 10	0.64 46	0.30 51
	CF	0.12 21	2.00 39	4.89 21	0.75 12	0.15 11	0.60 89	0.41 30
With dose apportionment	FOCE-I ODE	0.01 235	1.12 52	-	0.53 37	0.06 76	0.91 3579	0.01 54
	CF	0.01 NE	1.15 NE	-	0.54 NE	0.05 NE	0.85 NE	0.01 NE
Similar absorption rates	SAEM ODE	0.07 34	1.66 22	-	0.10 12	0.20 10	0.54 36	0.34 10
	CF	0.07 37	1.96 22	-	0.12 12	0.14 12	0.53 61	0.49 9

NE: not estimated

$\omega$ : between-subject standard deviation

\* Estimates that rely on the assumption that  $V_m = V_p$

Table IV. Population pharmacokinetic parameters of the parent drug and its active metabolite for the model without and with the genetic covariate: estimates and relative standard errors (in grey, %) using the SAEM algorithm in MONOLIX and encoding in closed form

	Without the genetic covariate (N=101)		With the genetic covariate (N=99)	
f	1.00	-	1.00	-
$\beta_{f,D} * (nmol^{-1})$	-0.02	28	-0.02	24
$F_p*$	0.85	2	0.87	2
$\beta_{F_p,D} * (nmol^{-1})$	-0.04	29	-0.06	27
$K_a (h^{-1})$	8.06	-	8.06	-
$V * (L)$	19.2	4	19.4	5
$CL_{po} * (L.h^{-1})$	0.84	11	0.67	11
$CL_{pm} * (L.h^{-1})$	1.94	5	2.09	5
$CL_{mo} * (L.h^{-1})$	0.46	6	0.50	7
$\beta_{CL_{mo},CYP2D6} * (log(L.h^{-1}))$	-	-	-0.42	40
$CL_{mp} * (L.h^{-1})$	0.09	12	0.09	12
$\omega_f*$	0.25	13	0.27	12
$\omega_{K_a}*$	1.50	21	1.41	25
$\omega_V*$	0.19	18	0.26	13
$\omega_{CL_{po}}*$	0.52	29	0.46	38
$\omega_{CL_{mo}}*$	0.51	8	0.50	8
$\gamma_{CL_{po}}*$	0.79	12	0.82	12
$b_p$	0.31	3	0.30	3
$a_m (nmol.L^{-1})$	66.9	14	66.5	14
$b_m$	0.06	9	0.06	9

$$V = V_p = V_m$$

$\omega$ : between-subject standard deviation

$\gamma$ : within-subject standard deviation

$a$ : additive coefficient in  $nmol.L^{-1}$

$b$ : multiplicative coefficient

$a_p$  was fixed to 0

\* Estimates that rely on the assumption that  $V_m = V_p$

675 **APPENDIX**

In all the equations below,  $C_p$  is the parent drug concentration in plasma and  $C_m$  is the active metabolite concentration in plasma following a single oral administration of a dose  $D$  of the parent drug.

The ordinary differential equation system and the corresponding closed form solution  
680 correspond to the last model on the right hand side of Figure 2, with similar absorption rates  $K_a = K_{ap} = K_{am}$ .

***Ordinary differential equation system***

$$\begin{aligned} \frac{dC_p}{dt} &= \frac{K_a f D F_p e^{-K_a t}}{V_p} - (k_{po} + k_{pm})C_p + k_{mp} \frac{V_m}{V_p} C_m \\ \frac{dC_m}{dt} &= \frac{K_a f D (1 - F_p) e^{-K_a t}}{V_m} - (k_{mo} + k_{mp})C_m + k_{pm} \frac{V_p}{V_m} C_p \end{aligned} \quad (4)$$

In the ordinary differential equation system (4),  $f$  is the fraction of dose after absorption,  $D$  is the dose,  $F_p$  is the fraction of parent reaching systemic circulation after absorption,  $K_a$  is the  
685 absorption constant for the parent and the metabolite,  $V_p$  is the volume of distribution for the parent,  $V_m$  is the volume of distribution for the metabolite,  $k_{po}$  is the parent rate constant of elimination by other pathways ( $= CL_{po}/V_p$ ),  $k_{pm}$  is the parent rate constant of transformation into the metabolite ( $= CL_{pm}/V_p$ ),  $k_{mo}$  is the metabolite rate constant of elimination by other pathways ( $= CL_{mo}/V_m$ ), and  $k_{mp}$  is the metabolite rate constant of back-transformation into the parent  
690 ( $= CL_{mp}/V_m$ ).

***Closed form solutions***

$$\begin{aligned} C_p &= \frac{fDK_a((E_2 - K_a) + k_{mp}(1 - F_p)/F_p)}{(V_p/F_p)(\lambda_1 - K_a)(\lambda_2 - K_a)} e^{-K_a t} + \frac{fDK_a((E_2 - \lambda_1) + k_{mp}(1 - F_p)/F_p)}{(V_p/F_p)(K_a - \lambda_1)(\lambda_2 - \lambda_1)} e^{-\lambda_1 t} \\ &+ \frac{fDK_a((E_2 - \lambda_2) + k_{mp}(1 - F_p)/F_p)}{(V_p/F_p)(K_a - \lambda_2)(\lambda_1 - \lambda_2)} e^{-\lambda_2 t} \end{aligned} \quad (5)$$

$$C_m = \frac{fDK_a((E_1 - K_a) + k_{pm}F_p/(1 - F_p))}{(V_m/(1 - F_p))(\lambda_1 - K_a)(\lambda_2 - K_a)}e^{-K_a t} + \frac{fDK_a((E_1 - \lambda_1) + k_{pm}F_p/(1 - F_p))}{(V_m/(1 - F_p))(K_a - \lambda_1)(\lambda_2 - \lambda_1)}e^{-\lambda_1 t} + \frac{fDK_a((E_1 - \lambda_2) + k_{pm}F_p/(1 - F_p))}{(V_m/(1 - F_p))(K_a - \lambda_2)(\lambda_1 - \lambda_2)}e^{-\lambda_2 t} \quad (6)$$

In both equations (5) and (6),  $E_1$  is the parent drug total rate constant of elimination ( $= k_{po} + k_{pm}$ ),  $E_2$  is the metabolite total rate constant of elimination ( $= k_{mo} + k_{mp}$ ), and  $\lambda_1$  and  $\lambda_2$  are the initial and terminal slopes of elimination, respectively defined in equations (7) and (8).

$$\lambda_1 = \frac{(E_1 + E_2) + \sqrt{(E_1 + E_2)^2 - 4(E_1 E_2 - k_{mp}k_{pm})}}{2} \quad (7)$$

$$\lambda_2 = \frac{(E_1 + E_2) - \sqrt{(E_1 + E_2)^2 - 4(E_1 E_2 - k_{mp}k_{pm})}}{2} \quad (8)$$

### ***Parameter identifiability***

From the model slopes, the following parameters may be identified:  $K_a$ ,  $\lambda_1$  and  $\lambda_2$ .

From the model intercepts, we can identify the following equations:

$$V = \frac{(E_2 - \lambda_1) + k_{mp}(1 - F_p)/F_p}{V_p/fF_p} \quad (9)$$

$$W = \frac{(E_2 - \lambda_2) + k_{mp}(1 - F_p)/F_p}{V_p/fF_p} \quad (10)$$

$$Y = \frac{(E_1 - \lambda_1) + k_{pm}F_p/(1 - F_p)}{V_m/f(1 - F_p)} \quad (11)$$

$$Z = \frac{(E_1 - \lambda_2) + k_{pm}F_p/(1 - F_p)}{V_m/f(1 - F_p)} \quad (12)$$

From (7) and (8) we can write:

$$\lambda_1 + \lambda_2 = E_1 + E_2 \quad (13)$$

$$\lambda_1 \lambda_2 = E_1 E_2 - k_{pm}(F_p/(1 - F_p))k_{mp}((1 - F_p)/F_p) \quad (14)$$

This yields a system of 6 equations, where V, W, Y and Z are four reals like  $\lambda_1$  and  $\lambda_2$ . We

can estimate the following parameters:  $V_p/fF_p$ ,  $V_m/f(1 - F_p)$ ,  $E_1 = k_{po} + k_{pm}$ ,  $E_2 = k_{mo} + k_{mp}$ ,

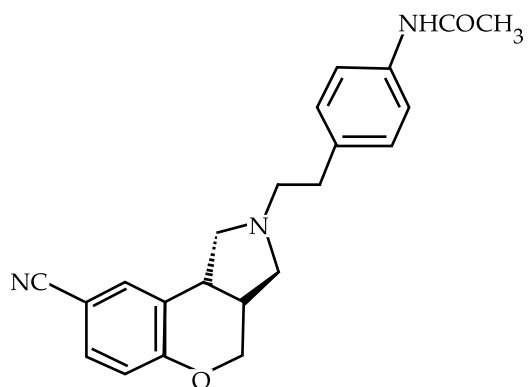
$k_{pm}F_p/(1 - F_p)$  and  $k_{mp}(1 - F_p)/F_p$ , with the following solutions:

$$\begin{aligned}
E_1 &= (\lambda_1 + \lambda_2 - \lambda_1 \lambda_2 / T_2 - T_1) / (1 - T_1 / T_2) \\
E_2 &= \lambda_1 + \lambda_2 - E_1 \\
k_{mp}(1 - F_p) / F_p &= (\lambda_2 - \lambda_1(W/V)) / (1 - W/V) - E_2 \\
k_{pm}F_p / (1 - F_p) &= (\lambda_2 - \lambda_1(Z/Y)) / (1 - Z/Y) - E_1 \\
V_p / fF_p &= \frac{(E_2 - \lambda_1) + k_{mp}(1 - F_p) / F_p}{V} \\
V_m / f(1 - F_p) &= \frac{(E_1 - \lambda_1) + k_{pm}F_p / (1 - F_p)}{Y}
\end{aligned} \tag{15}$$

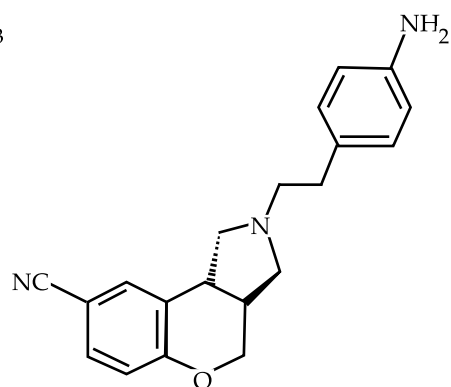
where  $T_1 = (\frac{\lambda_2}{W} - \frac{\lambda_1}{V}) / (\frac{1}{W} - \frac{1}{V})$  and  $T_2 = (\frac{\lambda_2}{Z} - \frac{\lambda_1}{Y}) / (\frac{1}{Z} - \frac{1}{Y})$ . Alternatively, the following parameterization may be used instead:

$$\begin{aligned}
&V_p / fF_p \\
&V_m / f(1 - F_p) \\
CL_{ptot} / fF_p &= E_1 \times V_p / fF_p \\
CL_{mtot} / f(1 - F_p) &= E_2 \times V_m / f(1 - F_p) \\
CL_{pm} / V_m &= k_{pm}V_p / V_m = k_{pm}F_p / (1 - F_p) \times V_p / fF_p \times f(1 - F_p) / V_m \\
CL_{mp} / V_p &= k_{mp}V_m / V_p = k_{mp}(1 - F_p) / F_p \times V_m / f(1 - F_p) \times fF_p / V_p
\end{aligned} \tag{16}$$

(a)



(b)



Without back-transformation

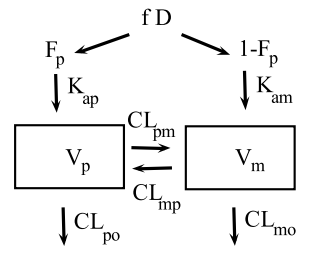
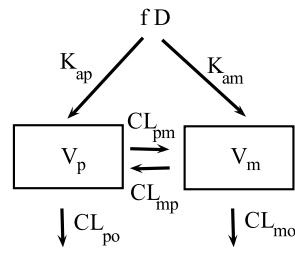
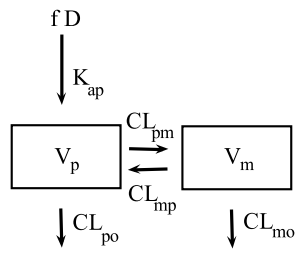
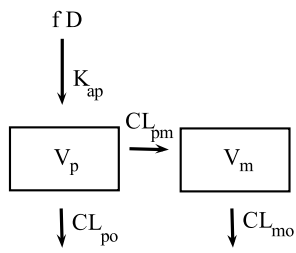
With back-transformation

Without first-pass effect

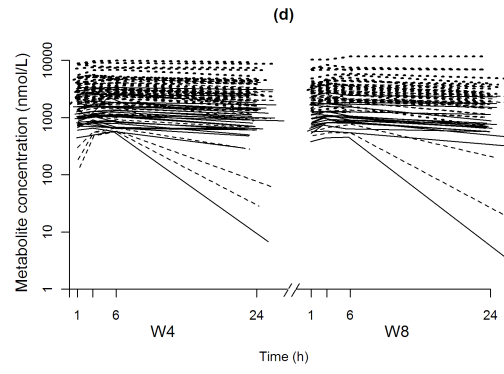
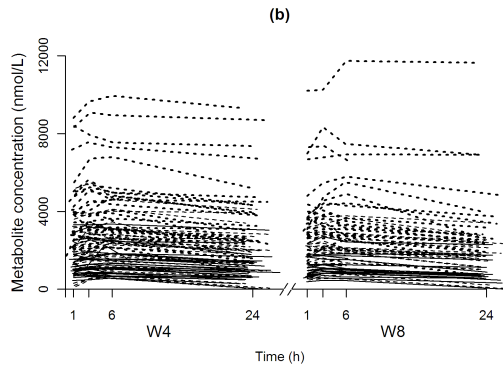
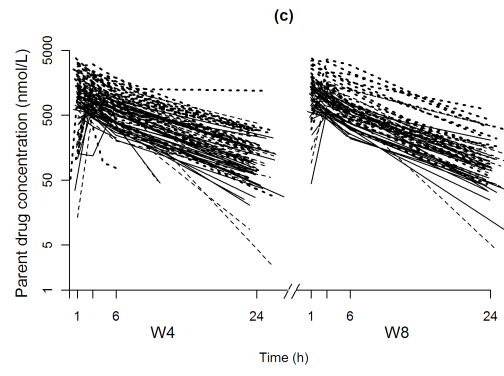
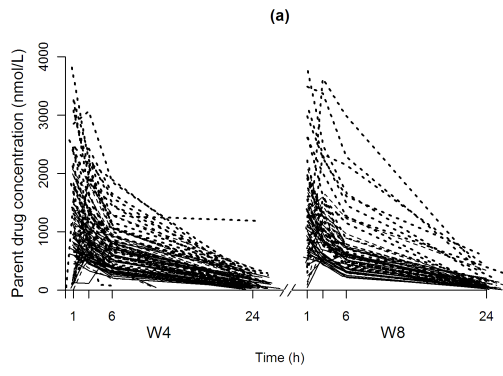
With first-pass effect

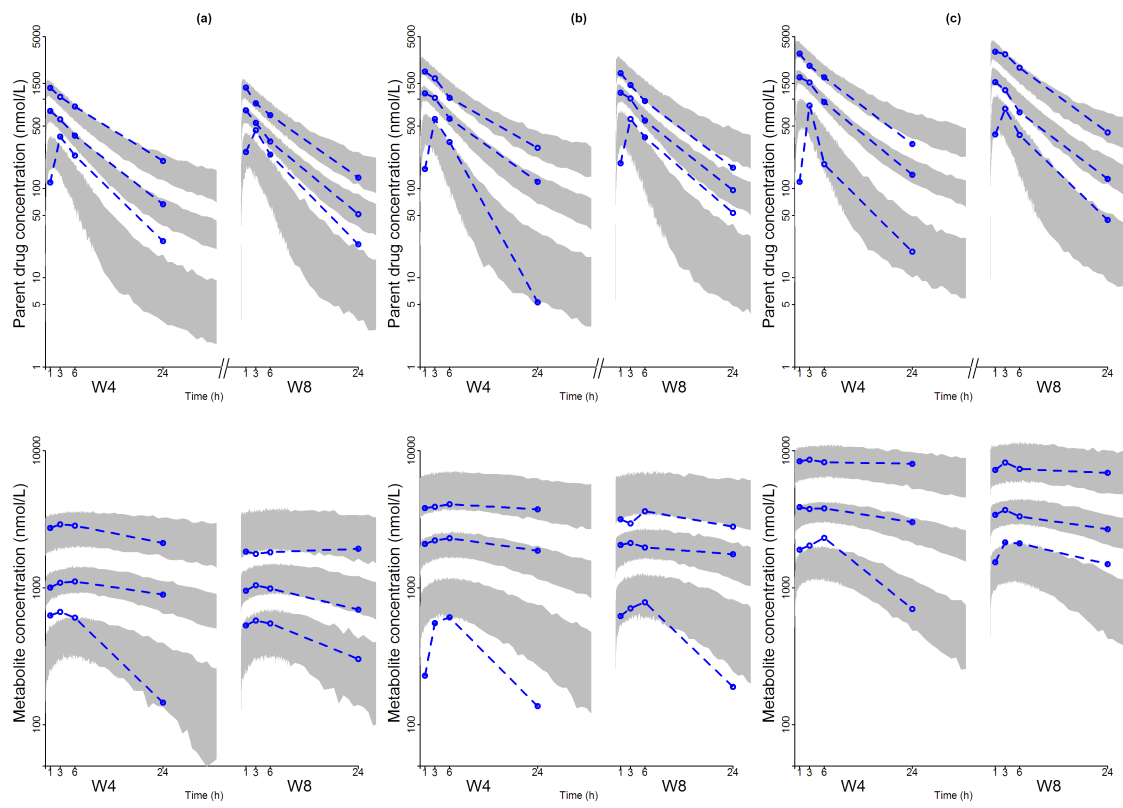
Without dose apportionment

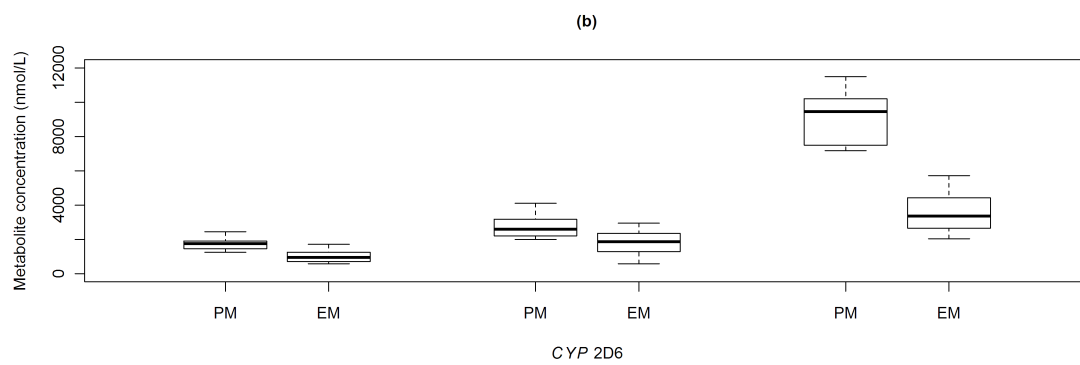
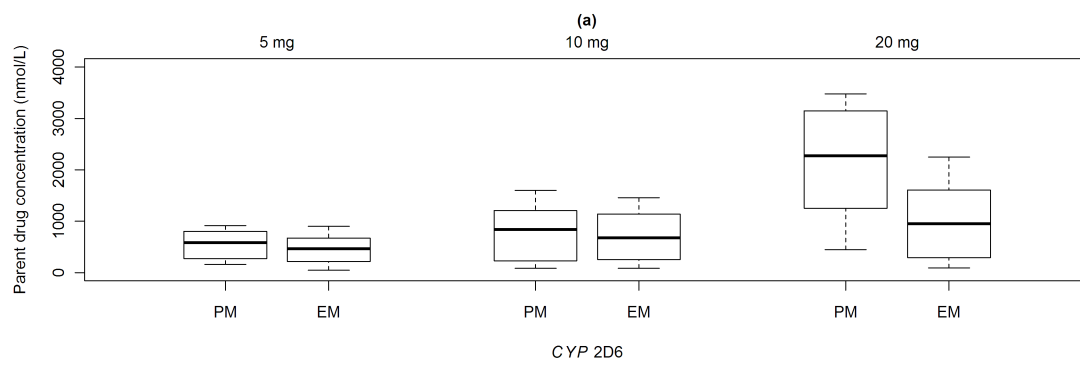
With dose apportionment

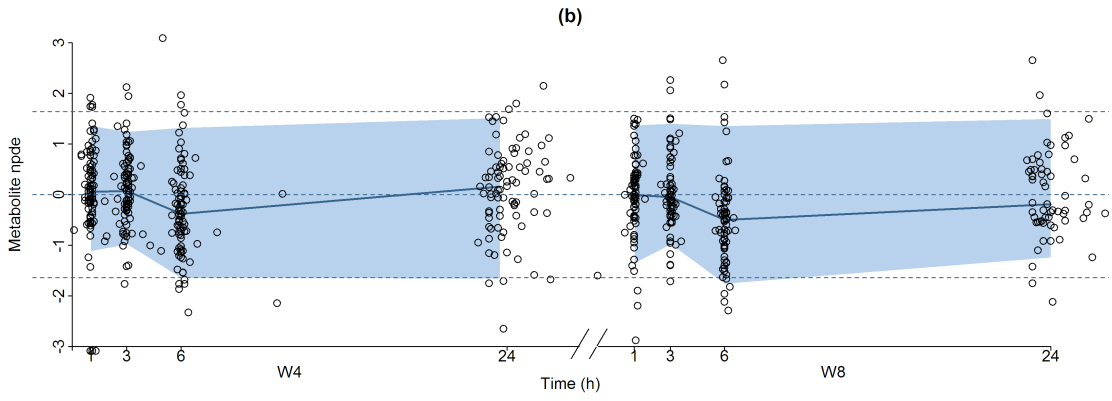
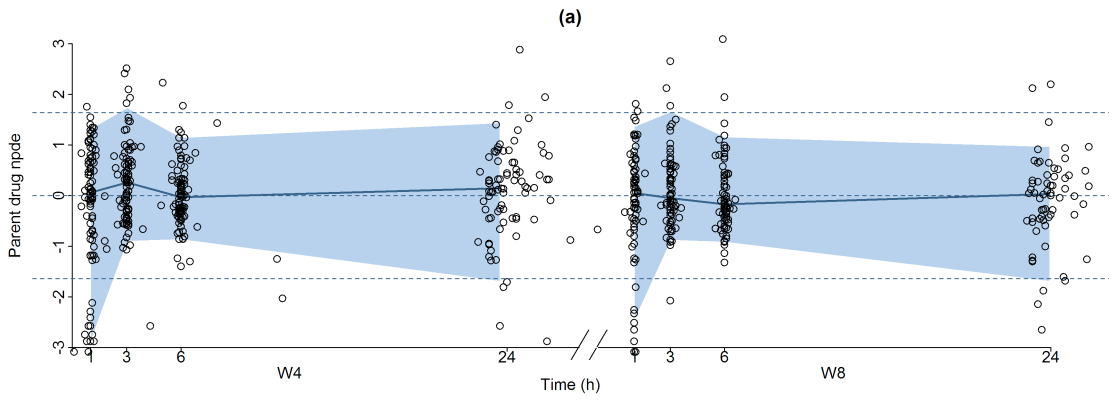


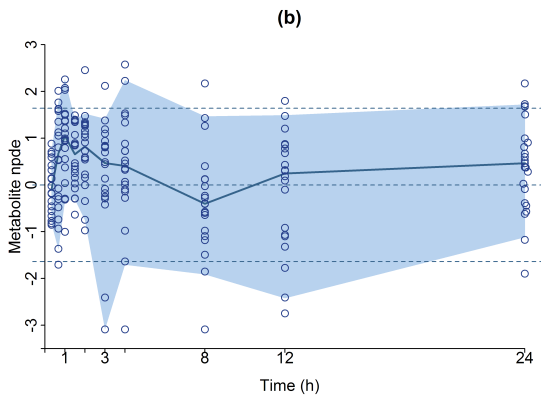
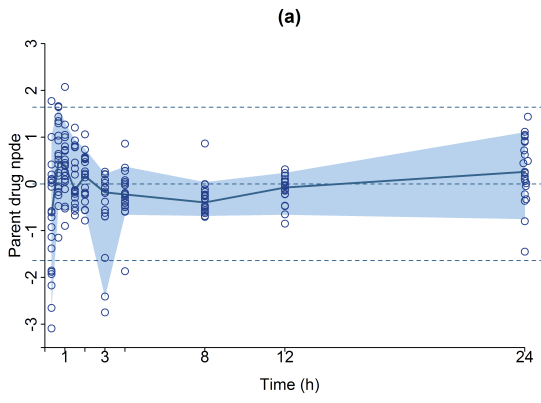
710











715

